

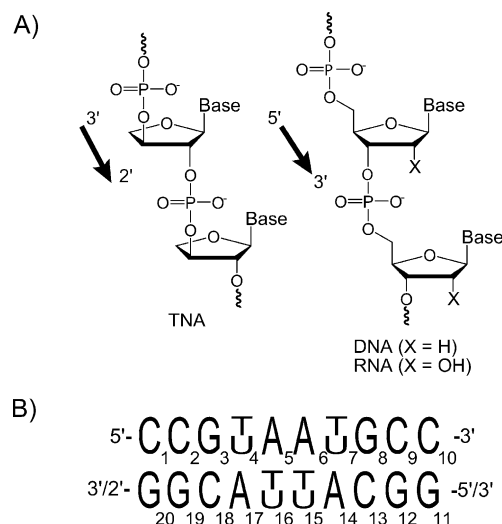


# Structural Insights into Conformation Differences between DNA/TNA and RNA/TNA Chimeric Duplexes

Irina Anosova,<sup>[a]</sup> Ewa A. Kowal,<sup>[b]</sup> Nicholas J. Sisco,<sup>[a]</sup> Sujay Sau,<sup>[c]</sup> Jen-yu Liao,<sup>[c]</sup> Saikat Bala,<sup>[c]</sup> Eriks Rozners,<sup>[d]</sup> Martin Egli,<sup>[b]</sup> John C. Chaput,<sup>[c]</sup> and Wade D. Van Horn<sup>\*[a]</sup>

Threose nucleic acid (TNA) is an artificial genetic polymer capable of heredity and evolution, and is studied in the context of RNA chemical etiology. It has a four-carbon threose backbone in place of the five-carbon ribose of natural nucleic acids, yet forms stable antiparallel complementary Watson–Crick homoduplexes and heteroduplexes with DNA and RNA. TNA base-pairs more favorably with RNA than with DNA but the reason is unknown. Here, we employed NMR, ITC, UV, and CD to probe the structural and dynamic properties of heteroduplexes of RNA/TNA and DNA/TNA. The results indicate that TNA templates the structure of heteroduplexes, thereby forcing an A-like helical geometry. NMR measurement of kinetic and thermodynamic parameters for individual base pair opening events reveal unexpected asymmetric “breathing” fluctuations of the DNA/TNA helix. The results suggest that DNA is unable to fully adapt to the conformational constraints of the rigid TNA backbone and that nucleic acid breathing dynamics are determined from both backbone and base contributions.

TNA ( $\alpha$ -L-(3'-2')-threofuranosyl nucleic acid) is an alternative genetic polymer in which the natural ribose sugar found in RNA has been replaced with an unnatural four-carbon sugar of  $\alpha$ -L-threose (Scheme 1A).<sup>[1]</sup> Despite a backbone repeat unit that is one atom shorter than that found in DNA and RNA, TNA is capable of adopting stable Watson–Crick duplex structures with itself and with complementary strands of DNA and RNA.<sup>[1a,2]</sup> The ability to exchange genetic information with RNA has raised significant interest in TNA as an RNA progenitor during the early stages of life on Earth.<sup>[3]</sup>



**Scheme 1.** A) Backbone constitutional structures of TNA, DNA, and RNA. B) Palindromic nucleotide sequences used in this study. In chimeric duplexes, TNA constitutes the bottom strand.

Relative to natural DNA and RNA, TNA has a sugar-phosphate backbone composed of quasi *trans*-diazial 3'-2' phosphodiester linkages, which places the phosphate groups in distinct relative positions.<sup>[4]</sup> Crystallographic analysis of B- and A-form duplexes with a single TNA nucleotide in an otherwise natural DNA strand revealed only minor effects on duplex geometry, base-pair stacking interactions, and the sugar pucker of neighboring native nucleotides.<sup>[5,6]</sup> In both structures, the threose sugar adopts a C4'-*exo*-pucker with a *trans*-diazial orientation of the 3'- and 2'-substituents. The preference for this sugar conformation (irrespective of the A- or B-form geometry) suggests that TNA has a limited range of sugar conformations compatible with Watson–Crick base pairing.

Nucleotide sequence can have dramatic effects on homo- and heteroduplex stability of both natural and artificial genetic polymers.<sup>[7]</sup> Hence, we focused on a single duplex sequence and examined the structural properties and the dynamics of Watson–Crick base pairing of a model palindromic decamer (Scheme 1B) of DNA/TNA and RNA/TNA heteroduplexes. The TNA strand was generated by solid-phase synthesis from chemically synthesized TNA phosphoramidites.<sup>[8]</sup> DNA and RNA homoduplexes were prepared and studied as a direct comparison to standard B- and A-form helices, respectively.

1D <sup>1</sup>H NMR spectra of the homo- and heteroduplexes indicate that all four helices form standard Watson–Crick interactions, as determined from the chemical shift and dispersion of the imino proton resonances (12–14 ppm, Figure S1 in the

[a] Dr. I. Anosova, N. J. Sisco, Prof. Dr. W. D. Van Horn  
School of Molecular Sciences and the Biodesign Institute  
Arizona State University  
551 E. University Dr., PSG-106, Tempe, AZ 85287 (USA)  
E-mail: wade.van.horn@asu.edu

[b] Dr. E. A. Kowal, Prof. Dr. M. Egli  
Department of Biochemistry, Vanderbilt University School of Medicine  
Robinson Research Building 868A, Nashville, TN 37232 (USA)

[c] Dr. S. Sau, J.-y. Liao, S. Bala, Prof. Dr. J. C. Chaput  
Department of Pharmaceutical Sciences, University of California Irvine  
147 Bison Modular, Building 515, Irvine, CA 92697 (USA)

[d] Prof. Dr. E. Rozners  
Department of Chemistry, Binghamton University  
State University of New York  
Science 2 Building 308, Binghamton, NY 13902 (USA)

Supporting information for this article can be found under <http://dx.doi.org/10.1002/cbic.201600349>.

Supporting Information). At low temperatures, each decamer had eight sharp imino proton resonances, representative of stable duplexes, with fraying exclusively at the termini. Imino proton NMR spectra of the DNA and RNA helices between 5 and 50 °C (Figure S2) indicated that the DNA structures had lower thermal stability than the RNA structures. Consistent with the NMR data, UV spectroscopy thermal denaturation curves yielded melting temperature ( $T_m$ ) values that were

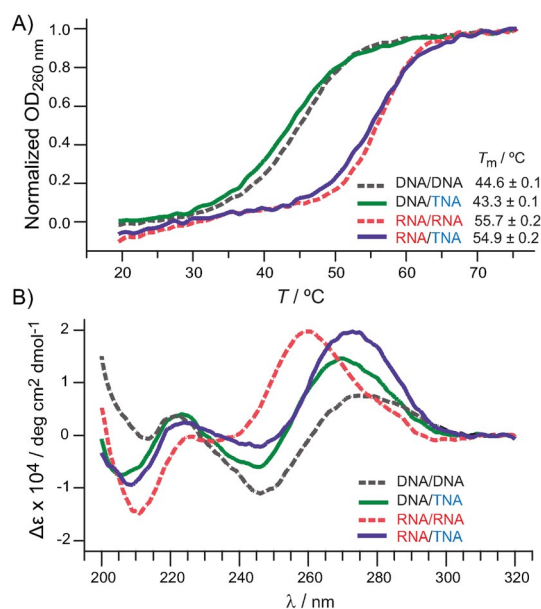


**Figure 1.** Thermal stability and CD analysis of model duplexes DNA/TNA, DNA/DNA, RNA/TNA, and RNA/RNA. A) Normalized UV-detected melting curves collected at 260 nm.  $T_m$  values are given in the lower right corner. B) Overlay of CD spectra at pH 7.0/25 °C. Data are mean residue molar ellipticity.

~10 °C lower for DNA/TNA and DNA/DNA helices than for RNA/TNA and RNA/RNA (Figure 1A).

Thermal denaturation studies showed similar in stabilities for each chimeric duplex and the corresponding homoduplex (Figure 1A). This observation is consistent with previous analysis on mixed-sequence TNA/RNA and TNA/DNA hetero- and homoduplexes.<sup>[1a]</sup> The  $T_m$  values are partly reflected by the thermodynamic parameters obtained by ITC (Table 1, and Figure S3). All duplexes had similar association stabilities with an average  $\Delta G$  of  $-43 \pm 3$  kJ mol<sup>-1</sup>. However, the dissociation constants ( $K_D$ ) differed significantly: much higher for DNA/TNA (135 nM) than for DNA/DNA (15 nM), RNA/RNA (12 nM) and RNA/TNA (45 nM). This suggests a degree of structural incompatibility or increased dynamics for DNA/TNA.

The CD spectra also reveal conformational differences between the homo- and heteroduplexes (Figure 1B). As expected,

Table 1. ITC thermodynamic parameters.				
	DNA/DNA	DNA/TNA	RNA/RNA	RNA/TNA
$K_D$ [nM]	$15.0 \pm 3.0$	$134.5 \pm 5.4$	$11.7 \pm 3.0$	$45.0 \pm 4.6$
$\Delta H$ [kJ mol <sup>-1</sup> ]	$-278 \pm 11$	$-258 \pm 16$	$-330 \pm 6$	$-240 \pm 5$
$\Delta G$ [kJ mol <sup>-1</sup> ]	$-44.8 \pm 0.5$	$-39.3 \pm 0.1$	$-45.4 \pm 0.6$	$-42.0 \pm 0.3$
$-T\Delta S$ [kJ mol <sup>-1</sup> ]	$234 \pm 11$	$219 \pm 16$	$284 \pm 6$	$198 \pm 4$

ed, the CD spectrum from DNA/DNA is typical of a standard B-form helix, with low mean residue molar ellipticity ( $\Delta\epsilon$ ) arising from lower chirality of the perpendicularly oriented base pairs (positive peak at 275 nm, negative peak at 245 nm). The RNA/RNA CD spectrum is consistent with an A-form helix (positive peak at 260 nm, negative peak near 210 nm). DNA/TNA and RNA/TNA exhibited  $\Delta\epsilon$  values comparable to that of RNA/RNA (maxima near 270 nm, minima at 245 nm, strong negative bands near 210 nm). This is consistent with an RNA-like A-form conformation.

Imino protons in NMR are very sensitive to nucleic-acid secondary structure.<sup>[9]</sup> We recorded <sup>1</sup>H,<sup>1</sup>H NOESY spectra for each construct in aqueous buffer at 15 °C and assigned the imino proton resonances (Figure 2A). As expected, imino protons for the termini (C1–G20 and C10–G11) were not observed due to their rapid exchange with water. However, all other imino protons were clearly identified. Consistent with their respective helical geometries, RNA (A-form) and DNA duplexes (B-form) yielded imino NOE crosspeaks with high and low peak intensities, respectively. In agreement with the CD analysis, the NMR imino regions of the RNA/TNA, and DNA/TNA duplex spectra are similar to the A-form RNA/RNA duplex (Figure 2A). This result is most easily observed by comparing the G3-T(U)4 and T(U)7-G8 NOESY cross peaks.

Estimated sequential imino distances for the G3-T(U)4 and T(U)7-G8 bases (5'→3') were calculated from NOE crosspeak intensities under the initial rate approximation<sup>[10]</sup> (Supporting Information). As expected, the distances are consistent with a B-form helix for DNA/DNA and A-like for RNA/RNA, RNA/TNA, and DNA/TNA (Figure 2A).<sup>[9]</sup> Taken together, these data indicate that TNA adopts A-like heteroduplex helices.

For a better understanding of the stability and dynamics of the TNA heteroduplexes, we measured the rate of single base pair breathing events by NMR. Breathing motions in nucleic acid polymers are accompanied by the exchange of base imino hydrogens with water protons in the aqueous surrounding.<sup>[11]</sup> We measured and analyzed imino proton solvent exchange rate constants ( $k_{ex}$ ) and estimated the individual base-pair stability in each of the four duplexes using solvent-exchange-based NMR methods (Figures 3A and S4).<sup>[12]</sup> The directionality of each duplex was assigned from <sup>1</sup>H,<sup>1</sup>H NOESY anomeric-aromatic proton walks and directional H1'-H6/H8 correlations.<sup>[13]</sup> Single-base-pair stability analysis was performed for C2–G19 through C9–G12. Terminal  $k_{ex}$  values were lower for RNA/RNA and RNA/TNA than for DNA/DNA and DNA/TNA (Figure 3A). Fraying in the RNA duplexes was limited to the terminal base-pairs of C1–G20 and C10–G11;  $k_{ex}$  values were uniformly low throughout the sequence, but with a slight increase in variability for RNA/TNA. With the exception of the penultimate base pairs, DNA/DNA also exhibited generally low flexibility in the core of the duplex structure, with  $k_{ex}$  comparable to RNA/RNA. However, the penultimate base-pair exchange rates rose symmetrically (~fivefold) over those observed in the core of the helix, consistent with symmetric, elevated motions at the duplex ends.

The DNA/TNA base-pair kinetics revealed a previously uncharacterized asymmetric terminal exchange: ~20 times higher

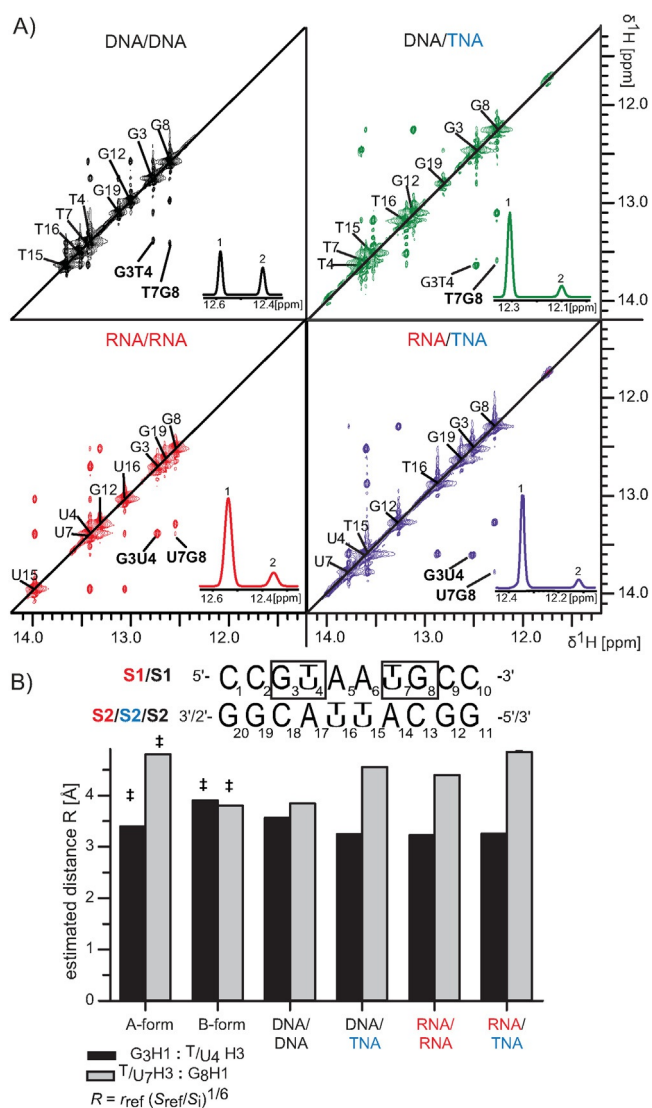


**Figure 2.** Conformational analysis of TNA heteroduplexes by solution NMR. A) Imino regions of  $^1\text{H}$ ,  $^1\text{H}$  NOESY spectra of hetero- and homoduplexes measured at 15 °C. Spectra were scaled for comparison. Diagonal peaks are assigned with the diagonal shown as black line. Sequential peaks G3–T/U4 and T/U7–G8 used in quantitative analysis are indicated, with their Gaussian-fitted direct dimension profiles in the lower right corner (1 and 2, respectively). B) Top: Boxes identify studied sequential bases. Bottom: estimated sequential  $^1\text{H}$ – $^1\text{H}$  distance ( $R$ ) of G3H1:T/U4H3 and T/U7H3:G8H1 (5'→3') compared to standard values of canonical A- and B-form DNA ( $\pm$ ). The strand identifiers are color coded according to the nucleic acid of origin.

$k_{\text{ex}}$  at the 5'/2'-end (C2–G19) than the rest of the helix, where  $k_{\text{ex}}$  values remained low and comparable to rates observed in the other constructs. Fraying at the 3'/3'-end was again solely at the terminal pair. Differences in the intramolecular dynamics of DNA/DNA and DNA/TNA were also observed for the duplexes, as differences in translational diffusion rates (measured by NMR), with the DNA/TNA diffusing slower (Figure S5). The significant terminal fraying of DNA/DNA and DNA/TNA might explain the observed differences in thermal stability between these and RNA/RNA and RNA/TNA. Surprisingly, TNA/DNA formed a dynamic, asymmetric duplex structure in solution. The experiments were recorded at buffer concentrations that allow multiple closing and opening base-pair events prior to

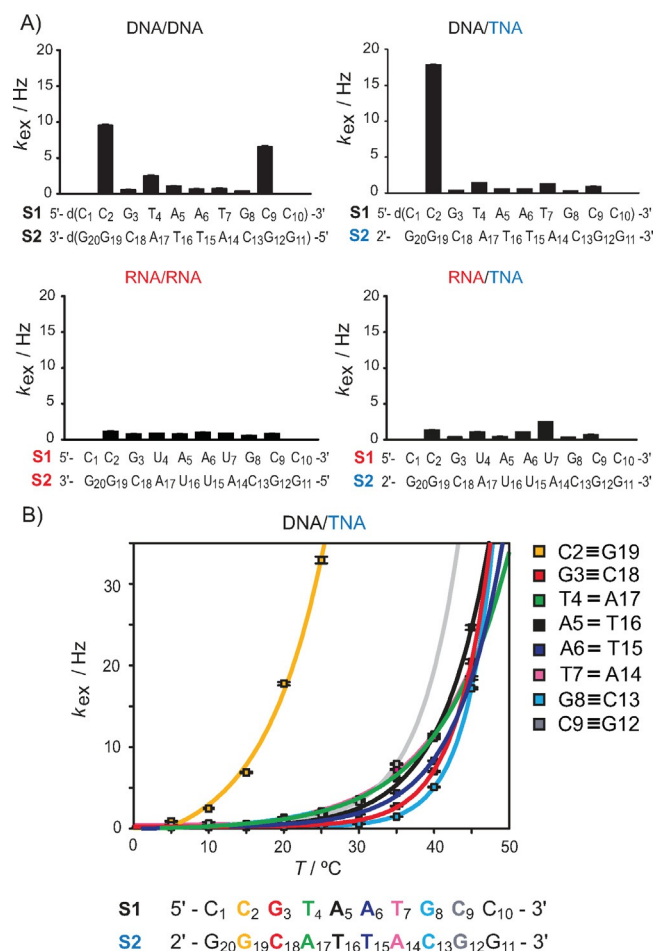


**Figure 3.** Individual base-pair stabilities in the four duplexes. A) Solvent exchange rates ( $k_{\text{ex}}$ ) of imino protons for individual base pairs at 20 °C (sequences shown below). B) Temperature dependence of  $k_{\text{ex}}$  for single base-pairs in DNA/TNA. The fits (lines) were obtained from Equation 6 in the Supporting Information.

imino proton exchange (EX2 regime). This indicates that the asymmetric distribution of DNA/TNA  $k_{\text{ex}}$  reflects increased flexibility of the 5'/2'-end. One carbon fewer per residue in the threose-linked strand presumably results in increased backbone rigidity. Our data suggest that, unlike RNA, DNA might be near the limit of its structural variability when paired with TNA. This is rooted in the phosphate group pitch differences of DNA (~6.8 Å), RNA (~6.0 Å) and TNA (~5.7 Å) caused by the sugar pucker. The high entropic costs for pucker adaptation increase with oligonucleotide length, thus possibly explaining the elevated  $K_D$  of the DNA/TNA duplex formation and limiting the duplex formation to relatively short polymers.

In order to investigate asymmetric base-pair breathing in DNA/TNA, we measured the individual base-pair imino proton exchange rates at different temperatures (Figure 3B).<sup>[14]</sup> As expected,  $k_{\text{ex}}$  for C2–G19 increased with temperature to the detection limit at 25 °C. Exchange rates for the other base pairs followed a much slower temperature-dependent exponential curve (detection limits  $\geq 40$  °C). By fitting the temperature dependent  $k_{\text{ex}}$  (Equation 6 in the Supporting Information), we extracted the enthalpy ( $\Delta H_{\text{Diss}}$ ) and entropy ( $\Delta S_{\text{Diss}}$ ) for single base-pair dissociations in the DNA/TNA duplex. The Gibbs free

**Table 2.** Thermodynamics of DNA/TNA duplex individual base-pair openings.<sup>[a]</sup>

DNA/ TNA <sup>[b]</sup>	$\Delta H_{\text{Diss}}$ [kJ mol <sup>-1</sup> ]	$\Delta S_{\text{Diss}}$ [J mol <sup>-1</sup> K <sup>-1</sup> ]	$\Delta G_{\text{Diss}}$ [kJ mol <sup>-1</sup> ]	$T\Delta S_{\text{Diss}}$ [kJ mol <sup>-1</sup> ]
C2≡G19	73 ± 8	198 ± 27	15 ± 11	58 ± 8
G3≡C18	145 ± 3	396 ± 9	29 ± 4	116 ± 3
T4=A17	42 ± 3	74 ± 10	20 ± 4	22 ± 3
A5=T16	82 ± 5	201 ± 17	23 ± 7	59 ± 5
A6=T15	84 ± 4	206 ± 12	24 ± 5	60 ± 3
T7=A14	44 ± 4	80 ± 15	21 ± 7	23 ± 4
G8≡C13	175 ± 1	490 ± 4	31 ± 2	144 ± 1
C9≡G12	112 ± 8	299 ± 27	24 ± 11	88 ± 8

[a] Data recorded at 20 °C. [b] TNA bases are in blue.

energy of the process ( $\Delta G_{\text{Diss}}$ ) was calculated according to the Gibbs–Helmholtz equation (Table 2).

The DNA/TNA thermodynamic data for single base-pair breathing events are similar to previously reported values for DNA and RNA duplexes, stem regions of RNA loops,<sup>[14]</sup> and imino exchange rates measured at elevated exchange catalyst concentrations.<sup>[15]</sup> The magnitude and sign of  $\Delta H_{\text{Diss}}$  suggest that the DNA/TNA base pairs were enthalpically stabilized. Higher values at the ends for  $\Delta H_{\text{Diss}}$ (GC) compared to  $\Delta H_{\text{Diss}}$ (AT) in the middle likely reflect the formation of all three hydrogen bonds between guanine and cytosine. Reported  $\Delta G_{\text{Diss}}$  for central bases in DNA duplexes are 24–32.6 kJ mol<sup>-1</sup>,<sup>[14b,15a]</sup> for DNA/TNA central pairs  $\Delta G_{\text{Diss}}$  was mostly at the lower end of this range. The asymmetry of duplex breathing was reflected by the distribution of  $\Delta G_{\text{Diss}}$ : central DNA/TNA base pairs showed comparable  $\Delta G_{\text{Diss}}$  values, whereas  $\Delta G_{\text{Diss}}$  (C2–G19) is consistent with the dynamic behavior and lower stability of the 5'/2' end.

In general,  $\Delta G_{\text{Diss}}$  for each base pair was far less than the absolute value of  $\Delta G$  for the heteroduplex formation measured by ITC, thus indicating that DNA/TNA heteroduplex stability is highly cooperative. The distribution of  $\Delta G_{\text{Diss}}$  values suggest that the opening of single DNA/TNA base pairs is primarily uncorrelated at 20 °C. Enthalpy–entropy compensation (i.e., variations in  $\Delta H_{\text{Diss}}$  and  $\Delta S_{\text{Diss}}$  to offset one another in order to allow biologically accessible  $\Delta G_{\text{Diss}}$ ) was observed for single base-pairs, thus suggesting that processes are involved in TNA/DNA stabilization are similar to those for RNA duplex melting. This effect was observed macroscopically in related systems,<sup>[16]</sup> and more recently was described at the single base-pair level in a dsRNA stem.<sup>[14a]</sup>

In summary, we have reported an extensive biophysical and thermodynamic characterization of base-pairing interactions between TNA and DNA and between TNA and RNA. Despite similar thermal and thermodynamic stabilities, TNA strongly favors an A-type helical geometry when paired with either DNA or RNA. Thermodynamic characterization of single base-pair opening events indicated that the higher stability of RNA/TNA base-pairing (over DNA/TNA) is attributable to asymmetric fraying at the 5'/2' terminus. This previously uncharacterized effect manifests itself at the macromolecular level as hydrodynamic differences between DNA/TNA and DNA/DNA. We suggest that this phenomenon is likely attributable to the inability

of DNA fully to adapt to the conformational constraints of a rigid TNA backbone. As a result, structural studies of DNA/TNA duplexes could prove challenging. These data also suggest that in addition to thermodynamic differences in stability between AT- and GC-rich nucleic acid segments, backbone contributions can significantly alter conformational fluctuations in double-stranded nucleic acid breathing.

## Acknowledgements

This work was supported by the DARPA Fold F(x) Program (N66001-14-2-4054) and National Institutes of Health (GM071461 to E.R.). We thank Prof. Dr. Harald Schwalbe and Dr. Hannah Steinert for helpful comments on imino proton exchange NMR and Prof. Dr. Jennifer Heemstra for helpful discussions.

**Keywords:** conformation analysis · DNA · nucleic acid dynamics · RNA evolution · TNA

- [1] a) K.-U. Schöning, P. Scholz, S. Guntha, X. Wu, R. Krishnamurthy, A. Eschenmoser, *Science* **2000**, *290*, 1347–1351; b) I. Anosova, E. A. Kowal, M. R. Dunn, J. C. Chaput, W. D. Van Horn, M. Egli, *Nucleic Acids Res.* **2016**, *44*, 1007–1021.
- [2] Y.-W. Yang, S. Zhang, E. O. McCullum, J. C. Chaput, *J. Mol. Evol.* **2007**, *65*, 289–295.
- [3] L. Orgel, *Science* **2000**, *290*, 1306–1307.
- [4] a) M.-O. Ebert, C. Mang, R. Krishnamurthy, A. Eschenmoser, B. Jaun, *J. Am. Chem. Soc.* **2008**, *130*, 15105–15115; b) M.-O. Ebert, B. Jaun, *Chem. Biodiversity* **2010**, *7*, 2103–2128.
- [5] C. J. Wilds, Z. Wawrzak, R. Krishnamurthy, A. Eschenmoser, M. Egli, *J. Am. Chem. Soc.* **2002**, *124*, 13716–13721.
- [6] P. S. Pallan, C. J. Wilds, Z. Wawrzak, R. Krishnamurthy, A. Eschenmoser, M. Egli, *Angew. Chem. Int. Ed.* **2003**, *42*, 5893–5895; *Angew. Chem.* **2003**, *115*, 6073–6075.
- [7] K.-U. Schöning, P. Scholz, X. Wu, S. Guntha, G. Delgado, R. Krishnamurthy, A. Eschenmoser, *Helv. Chim. Acta* **2002**, *85*, 4111–4153.
- [8] S. P. Sau, N. E. Fahmi, J.-Y. Liao, S. Bala, J. C. Chaput, *J. Org. Chem.* **2016**, *81*, 2302–2307.
- [9] K. Wüthrich, *NMR of Proteins and Nucleic Acids*, Wiley, New York, **1986**.
- [10] J. Cavanagh, W. J. Fairbrother, A. G. Plamer III, M. Rance, N. Skelton, *Protein NMR Spectroscopy. Principles and Practice.*, Elsevier, Amsterdam, **2007**.
- [11] M. Guéron, J.-L. Leroy, *Methods Enzymol.* **1995**, *261*, 383–413.
- [12] “NMR Analysis of Base-Pair Opening Kinetics in DNA”, M. W. Szulik, M. Voehler, M. P. Stone in *Current Protocols Nucleic Acid Chem.* **2014**, *59*, Unit 7.20.
- [13] a) R. Boelens, R. M. Scheek, K. Dijkstra, R. Kaptein, *J. Magn. Reson.* **1985**, *62*, 378–386; b) B. Fürtig, C. Richter, J. Wöhnert, H. Schwalbe, *ChemBioChem* **2003**, *4*, 936–962.
- [14] a) J. Rinnenthal, B. Klinkert, F. Narberhaus, H. Schwalbe, *Nucleic Acids Res.* **2010**, *38*, 3834–3847; b) H. S. Steinert, J. Rinnenthal, H. Schwalbe, *Biophys. J.* **2012**, *102*, 2564–2574; c) D. Wagner, J. Rinnenthal, F. Narberhaus, H. Schwalbe, *Nucleic Acids Res.* **2015**, *43*, 5572–5585.
- [15] a) C. Chen, I. M. Russu, *Biophys. J.* **2004**, *87*, 2545–2551; b) Y. Huang, X. Weng, I. M. Russu, *Biochemistry* **2011**, *50*, 1857–1863; c) E. Folta-Stogniew, I. M. Russu, *Biochemistry* **1994**, *33*, 11016–11024; d) J. G. Moe, I. M. Russu, *Biochemistry* **1992**, *31*, 8421–8428.
- [16] a) H. Lis, N. Sharon, *Chem. Rev.* **1998**, *98*, 637–674; b) L. Liu, C. Yang, Q.-X. Guo, *Biophys. Chem.* **2000**, *84*, 239–251.

Manuscript received: June 20, 2016

Accepted article published: June 27, 2016

Final article published: July 29, 2016

# CHEMBIOCHEM

## Supporting Information

### **Structural Insights into Conformation Differences between DNA/TNA and RNA/TNA Chimeric Duplexes**

Irina Anosova,<sup>[a]</sup> Ewa A. Kowal,<sup>[b]</sup> Nicholas J. Sisco,<sup>[a]</sup> Sujay Sau,<sup>[c]</sup> Jen-yu Liao,<sup>[c]</sup> Saikat Bala,<sup>[c]</sup> Eriks Rozners,<sup>[d]</sup> Martin Egli,<sup>[b]</sup> John C. Chaput,<sup>[c]</sup> and Wade D. Van Horn<sup>\*[a]</sup>

cbic\_201600349\_sm\_miscellaneous\_information.pdf

## **MATERIALS AND METHODS**

### **Oligonucleotides.**

DNA and RNA oligonucleotides were purchased desalted in required quantities from Integrated DNA Technologies (IDT, IDTDNA.com). TNA oligonucleotides were prepared on an automated ABI 3400 DNA synthesizer using chemically synthesized phosphoramidite monomers as described previously.<sup>[1]</sup> All oligonucleotides were PAGE purified and desalted into ddH<sub>2</sub>O. Concentration of the oligonucleotides was determined by absorbance at 260 nm using Beer's Law. For TNA, the extinction coefficient of DNA was used. Oligonucleotide single strands were mixed at 1:1 molar ratios, lyophilized overnight and taken up in the required experimental buffer. To form the duplexes, prior to conducting experiments the mixtures were heated for 5 min at 95 °C and let slowly cool down at room temperature for 15 minutes.

### **UV Absorbance Melting Studies.**

The oligonucleotide duplexes were prepared as described above. For each duplex, absorption at 260 nm vs. temperature profiles were collected on Varian Cary 100 Bio spectrophotometer (Varian Associates, Palo Alto, CA). The concentrations of the duplexes were set to 2 μM. Samples were prepared in a solution containing 0.1 M NaCl, 10 mM sodium phosphate and 50 μM Na<sub>2</sub>EDTA (pH 7.0). The temperature was increased from 10 to 85 °C for each duplex at a rate of 1.0 °C/min. For clarity, only points between 20 and 75 °C were used for analysis. Absorbance raw data was normalized to 75 °C values, initially fitted to a four parameter sigmoid curve using SigmaPlot™ 12.0 software, and normalized to the fit. The  $T_m$  values were determined from the second round of fitting (four parameter sigmoid fit) on the normalized data.

### **Circular Dichroism.**

The oligonucleotide duplexes were prepared as described above. The samples were prepared at ~ 10 μM concentration in 1 mL of 0.1 M NaCl, 10 mM sodium phosphate and 50 μM Na<sub>2</sub>EDTA (pH 7.0). Data was acquired at room temperature in 0.2 cm path length cuvette on a Jasco 710 spectropolarimeter (Jasco, Inc., Easton, MD) with a response time of 2 s, a scan rate of 100 nm/min, and step resolution of 1 nm across a wavelength of 200 – 320 nm with accumulation of 4 scans. A blank data set containing only buffer was

recorded at the same conditions and subtracted from the results prior to analysis. The data was converted to mean residue molar ellipticity using standard equations and analyzed with SigmaPlot™ 12.0 software.

### **Isothermal titration calorimetry (ITC).**

ITC experiments were done on a MicroCal iTC200 instrument using 50 mM potassium phosphate buffer at pH 7.4 containing 2 mM MgCl<sub>2</sub>, 90 mM KCl, 10 mM NaCl at 25 °C. 2.4 μL aliquots of one strand solution (100-125 μM) were sequentially injected from a 40 μL rotating syringe (500 rpm) into 200 μL of solution of the complementary strand (9-10 μM). The duration of each injection was 4.8 sec and the delay between injections was 350 sec. Data were analyzed using MicroCal PEAQ-ITC Analysis Software.1.0.0.1259.

### **NMR Spectroscopy.**

NMR spectra were recorded on nucleic acid complexes with 1:1 molar ratio of oligonucleotide strands in 50 mM sodium arsenate (pH 7.0), 2% v/v deuterium oxide aqueous buffer at following complex concentrations: DNA/DNA 2.7 mM (5 mm Shigemi tube), RNA/RNA 1.3 mM (3 mm standard tube), DNA/TNA and RNA/TNA 0.89 mM (4 mm Shigemi tube). The duplexes were prepared and annealed as described above. Experiments were performed on Bruker 850 MHz spectrometer equipped with a 5 mm TCI CryoProbe, Avance III HD console and pulse field gradients. The temperature of the spectrometer was calibrated using 99.8 % methanol-d<sub>4</sub>.<sup>[2]</sup> Samples were allowed to equilibrate at a given temperature for at least 5 min prior to acquisition. NMR spectra were processed and analyzed using Bruker TopSpin 3.2 and 3.5 and CcpNMR Analysis 2.3 software. All spectra were scaled by their noise levels prior to comparative investigations.

### **Resonance assignment.**

One dimensional <sup>1</sup>H experiments were acquired at 15 °C using a 1D pulse sequence with water suppression by excitation sculpting with gradients at standard parameters and 16384 points resolution. Two-dimensional <sup>1</sup>H, <sup>1</sup>H - Nuclear Overhauser effect Spectroscopy (NOESY) data was recorded at 15 °C with 150 ms mixing time in phase sensitive mode utilizing water suppression by excitation sculpting with gradients. 512 points were recorded in *t*<sub>1</sub> and 4096 points were recorded in *t*<sub>2</sub> dimension. Imino proton resonances were assigned using standard techniques<sup>[3]</sup>. Additionally, data from a natural abundance <sup>15</sup>N-heteronuclear single

quantum coherence (HSQC) spectra were used in assignment. This data was acquired in a phase sensitive mode using Echo/Antiecho–TPPI protocol with gradient selection and decoupling during acquisition, and recorded at 10 °C or 15 °C with 256 points in  $t_1$  and 2048 points in  $t_2$ . The directionality of the duplexes was assigned from anomeric–aromatic walks on the same  $^1\text{H}$ - $^1\text{H}$  NOESY spectra as described in references [3-4], utilizing directional H6/H8 base to H1' sugar correlations. Additional information was retrieved from natural abundance  $^{13}\text{C}$ –HSQC spectra acquired in a phase sensitive mode using Echo/Antiecho –TPPI acquisition mode with gradient coherence selection and decoupling during acquisition, recorded at 20 °C with 256 points in  $t_1$  and 2048 points in  $t_2$ .

### **Estimation of interproton distances from NOE.**

Distances between sequential protons were estimated from their cross peak intensities in  $^1\text{H}$ ,  $^1\text{H}$  – NOESY spectra used for assignments, applying the initial rate approximation and the following equation<sup>[5]</sup>:

$$R = r_{ref} \left( \frac{S_{ref}}{S_i} \right)^{1/6}, \quad (1)$$

where  $R$  is the estimated distance,  $r_{ref}$  is the known interproton distance between two neighboring protons,  $S_{ref}$  is the corresponding intensity of the reference cross-peak in the spectra and  $S_i$  is the intensity of the cross-peak of interest. As reference interproton distance ( $r_{ref}$ ), the H5-H6 distance in cytosine bases, which is approximately 2.43 Å<sup>[6]</sup>, was employed. As intrinsic reference intensity ( $S_{ref}$ ), the averaged intensity of C<sub>13</sub> and C<sub>18</sub> H5-H6 cross peaks in each respective spectrum was utilized. All peaks were fitted to a Gaussian line shape prior to analysis, using CcpNMR Analysis 2.3 software. The standard deviation was extracted as the error on intensity fit and propagated according to the standard protocols. The final errors constitute less than 1% of the estimated distance values. For comparison previously experimentally determined interproton distances in standard A-form and B-form helices were used<sup>[7]</sup>.

### **NMR translational diffusion measurements.**

NMR translational diffusion measurements were carried out using a pulse sequence with longitudinal-eddy-current delay and bipolar gradient pulses, which is available as a standard Bruker pulse *ledbpgp2s* program. Sixteen transients were acquired with 2048  $^1\text{H}$  points and a spectral width of 12 ppm centered at 4.701 ppm. As experimental parameters for the Stejskal-Tanner diffusion, the translational diffusion delay of 110

ms, gradient recovery delay of 2 ms, and gradient pulse duration of 2 ms were applied using a 20 point linear ramp from 2% and 95% of the gradient strength. The maximum gradient strength was calibrated using a Bruker doped water sample containing 0.1 mg/mL GdCl<sub>3</sub> in D<sub>2</sub>O, 1% H<sub>2</sub>O and 0.1% <sup>13</sup>CH<sub>3</sub>OH to a value of 54.11 G cm<sup>-1</sup> at 10 A.

The data was processed in Topspin 3.5 and analyzed with MATLAB R2015a (MathWorks). The integrated signal intensities were plotted as a function of G/cm and fit for initial signal intensity and the translational diffusion coefficient with the nonlinear *nlinfit* function to the Stejskal-Tanner NMR diffusion equation for bipolar gradients, which correlates the measured signal intensity to the translational diffusion coefficient according to the following equation<sup>[8]</sup>:

$$I = I_0 e^{-D_t(\gamma g \delta)^2(\Delta - \frac{\delta - \tau}{2})}, \quad (2)$$

where  $I$  is the relative intensity,  $I_0$  is the initial signal intensity,  $\delta$  is the gradient duration,  $\Delta$  is the Stejskal-Tanner diffusion delay,  $g$  is the gradient strength,  $\tau$  is the gradient recovery delay,  $\gamma$  is the gyromagnetic ratio of proton, and  $D_t$  is the translational diffusion coefficient.

### **Inversion recovery experiments.**

NMR experiments were recorded on the oligonucleotide duplexes in aqueous buffer, described above. The sets of experiments were recorded at 20 °C for DNA/DNA, DNA/TNA, RNA/RNA and RNA/TNA duplexes. For DNA/TNA sample, additionally, sets of experiments at 5 °C, 10 °C, 15 °C, 25 °C, 30 °C, 35 °C, 40 °C and 45 °C were recorded and analyzed.

Solvent exchange rates of imino protons at given temperatures were determined at  $B_0 = 20$  T (850 MHz) using a set of experiments optimized for high Q-probes and high water contents, utilizing 16384 point resolution and pulse sequences described elsewhere<sup>[9]</sup>. This method included determination of water longitudinal relaxation rate ( $R_{1w}$ ) utilizing optimized saturation recovery experiment with 18 variable exchange time delays ranging from 5 ms to 17 s. Longitudinal relaxation of imino protons ( $R_{1n}$ ) was measured indirectly as a sum of the actual longitudinal imino proton relaxation rate ( $R_1$ ) and their solvent exchange rate ( $k_{ex}$ ) from a standard pseudo two dimensional inversion recovery setup with binominal water suppression and variable relaxation delays. The number of points and durations of delays were optimized for each complex. 24 points were used in case of DNA-based duplexes (1 ms to 15 s for DNA/TNA and

1ms to 8 sec for DNA/DNA), 20 points ranging from 1 ms to 10 s were used in case of RNA/RNA, and 18 points ranging from 1 ms to 8 s were utilized in for RNA/TNA. The majority of delays was clustered in the first half of the curve to unambiguously determine the profiles of relaxation curves. Determination of proton exchange rates ( $k_{ex}$ ) was performed using selective inversion recovery setup, recorded as a pseudo two dimensional experiment with 24 points and variable recovery delays. The delays were optimized for each complex and ranged from 1 ms to 15 s for DNA-based duplexes and from 1 ms to 17 s for RNA-based oligonucleotide complexes. To unambiguously define the saturation recovery profiles, the majority of the delays was distributed through the first third of the curve. Water inversion efficiency factor ( $E$ ) was measured separately as a function of peak areas under the water signal before and after inversion, utilizing the same pulse sequence as for determination of imino proton exchange rate with no variable delay and immediate acquisition after the read-out pulse. Since the relative size of the investigated duplexes is rather low, the inter scan relaxation delay  $d_1$  was set each time to 20 sec for all experiments to allow complete relaxation of the samples between the scans.

For determination of  $R_{1w}$  and  $R_{1n}$ , the respective spectra were baseline corrected in each scan and the area under individual peaks was fitted to the exponential equation:

$$A = \alpha + \beta e^{\frac{-t}{T_{1n}}} \quad (3),$$

where  $A$  is the area under the peak,  $t$  is the respective experimental relaxation delay,  $T_{1n}$  is the longitudinal relaxation time in sec and  $\alpha$  and  $\beta$  are constants. Nonlinear least squared method was used. The respective relaxation rates ( $R_{1n}$ ) were obtained from

$$R_{1n} = \frac{1}{T_{1n}} \quad (4).$$

The inversion - recovery profiles of exchangeable protons were fitted subsequently to the following equation:

$$\frac{I(t)}{I_0} = 1 - E \times k_{ex} / (R_{1w} - R_{1n}) \times (e^{-R_{1n} \times t} - e^{-R_{1w} \times t}) \quad (5),$$

where  $I(t)$  is the intensity of the peak at exchange time  $t$ ,  $I_0$  is the intensity of the peak at equilibrium,  $E$  the efficiency factor of water inversion determined experimentally,  $k_{ex}$  the imino proton solvent exchange rate constant,  $R_{1w}$  the longitudinal relaxation rates of water and  $R_{1n}$  the sum of imino proton longitudinal

relaxation rate and its solvent exchange rate respectively. For this analysis, the intensities of each peak in the corresponding baseline corrected experiments were utilized.

All data was fitted with MATLAB R2014a (MathWorks) software using nonlinear fit and standard algorithms. Standard deviation was calculated as the error on the fit.

### **Imino proton solvent exchange rate analysis.**

The method and theory for thermodynamic analysis of base pair stability utilizing NMR-detected solvent exchange rates of imino protons at varying temperature, is extensively described elsewhere<sup>[10]</sup>. Here in brief.

Imino proton exchange rate analysis at varying temperatures was performed for the DNA/TNA sample. Given that at the working buffer concentrations and known thermal stability of the heteroduplex, the imino proton exchange could be described by a two state imino proton exchange model<sup>[10a, 11]</sup> and EX2 exchange regime, the apparent rate constants ( $k_{ex}$ ) at each temperature point were determined at conditions and utilizing the method described above. To obtain the enthalpy ( $\Delta H_{Diss}$ ) and entropy ( $\Delta S_{Diss}$ ) of DNA/TNA base pair dissociation the  $k_{ex}$  temperature dependent data for every imino proton resonance was fitted to the following equation:

$$k_{ex}(T) = \frac{(k_B T/h) \times e^{\frac{-(\Delta H_{TR} - T\Delta S_{TR})}{RT}}}{1 + e^{\frac{(\Delta H_{Diss} - T\Delta S_{Diss})}{RT}}} + d(T) \quad (6),$$

where  $k_{ex}(T)$  is the apparent imino proton exchange rate constant at varying temperature,  $T$  is the respective temperature in Kelvin,  $k_B$  is the Boltzmann constant,  $h$  is the Planck constant and  $R$  is the universal gas constant.  $\Delta H_{TR}$  and  $\Delta S_{TR}$  describe, respectively, the enthalpy and entropy of the transition state of the imino proton transition from the nucleobase in the completely open state to water, catalyzed by the proton acceptor in the buffer. Since inversion recovery experiments could include artefacts caused by dipolar cross-relaxation, parameter  $d$  was used to account for these effects. The equation was fitted with MATLAB R2014a (MathWorks) software using standard algorithms.  $\Delta H_{Diss}$  and  $\Delta S_{Diss}$  were allowed to adjust freely. Based on previously published work<sup>[10c]</sup>,  $d$  was fixed to the range 0 to 12 Hz. Gibbs free energy of base-pair dissociation ( $\Delta G_{Diss}$ ) at 20 °C was calculated according to the Gibbs-Helmholtz equation:

$$\Delta G_{Diss} = \Delta H_{Diss} - T\Delta S_{Diss} \quad (7).$$

Standard deviation was calculated as error on the fit. For  $T\Delta S_{Diss}$  and  $\Delta G_{Diss}$  it was propagated using standard error propagation protocols.

Thermodynamic parameters of the transition state of the imino proton transition in completely open state from base to water ( $\Delta H_{TR}$  and  $\Delta S_{TR}$ ) were derived from temperature dependencies of imino proton exchange rates of guanosine-5'-triphosphate (GTP) and thymidine-5'-triphosphate (dTTP) mononucleoside triphosphates based on previously published methods [10a, 10b]. GTP sodium salt hydrate (Sigma Aldrich, #T0251) and dTTP sodium salt (Sigma Aldrich, #G8877) were both diluted at two concentrations 2.5 mM NTP in 12.5 mM sodium arsenate (pH 7.0), 2% v/v deuterium oxide aqueous buffer and 1.25 mM NTP in 6.25 mM sodium arsenate (pH 7.0), 2% v/v deuterium oxide aqueous buffer. A set of one dimensional  $^1\text{H}$  NMR experiments was recorded for each condition, using a pulse program with short gradient delays, optimized for detection of imino – proton signal in an open base, at temperature range 4 to 10 °C with a pitch of 1 °C. The spectra were baseline corrected, phased and the line width of imino signals was obtained from their Lorentzian deconvolution using Bruker TopSpin 3.2. The exchange rate constant values ( $k_{ex}$ ) were determined from the signal line widths using the following equation:

$$k_{exNTP} = \Delta\nu\pi - R_2 - R_{2(B_0)} \quad (8),$$

where  $\Delta\nu$  is the line width of the dTTP or GTP imino signals at half height,  $R_2$  represents the spin-spin relaxation rate constant of the imino resonance, and  $R_{2(B_0)}$  corresponds to line broadening caused by  $B_0$  field inhomogeneities. The contribution of  $R_2$  relaxation and  $R_{2(B_0)}$  were considered very small in comparison to the contribution of  $k_{exNTP}$  to the imino line width and were neglected.

To account for the differences in diffusion of full length DNA/TNA heteroduplex and mononucleoside triphosphates,  $k_{exNTP}$  values were diffusion corrected, according to equation

$$k'_{exNTP} = \frac{\left(1 + \sqrt[3]{\frac{M_{cat}}{M_{DNA/TNA}}}\right)}{\left(1 + \sqrt[3]{\frac{M_{cat}}{M_{NTP}}}\right)} \quad (9),$$

where  $k'_{exNTP}$  is the diffusion corrected value of the imino proton exchange rate constant at each condition and  $M_{cat}$ ,  $M_{DNA/TNA}$ ,  $M_{NTP}$  are the molecular masses of the buffer catalyst ( $\text{HAsO}_4^{2-}$ ), the DNA/TNA heteroduplex and mononucleoside triphosphate, respectively. Subsequently,  $k'_{exNTP}$  values were extrapolated for each nucleoside triphosphate to 50 mM arsenate buffer concentrations to result in

$k'_{exNTP\_50mMAs} \cdot \ln(k'_{exNTP\_50mMAs}/T)$  was plotted against  $T$ , where  $T$  is the measurement temperature in Kelvin.

Finally, using Eyring formalism,  $\Delta H_{TR}$  and  $\Delta S_{TR}$  were obtained from fitting the data to the following equation:

$$\ln\left(\frac{k'_{exNTP\_50mMAs}}{T}\right) = -\frac{\Delta H_{TR}}{R} \frac{1}{T} + \frac{\Delta S_{TR}}{R} - \ln\left(\frac{h}{k_B}\right) \quad (10),$$

where  $k'_{exNTP\_50mMAs}$  is the extrapolated diffusion corrected imino proton exchange rate constant at 50 mM sodium arsenate buffer concentration,  $T$  is the temperature in Kelvin,  $R$  is the universal gas constant,  $h$  is the Planck constant and  $k_B$  is the Boltzmann constant. The data was fitted with MATLAB R2014a (MathWorks) software using nonlinear fit and standard algorithms. Standard deviation was calculated as the error on the fit. At used conditions, the following values for  $\Delta H_{TR}$  and  $\Delta S_{TR}$  were obtained:

$\Delta H_{TR}(\text{GTP}) = 30.39 \pm 1.34$  kJ/mol and  $\Delta S_{TR}(\text{GTP}) = -66.38 \pm 4.77$  J/molK;  $\Delta H_{TR}(\text{dTTP}) = 41.38 \pm 3.27$  kJ/mol and  $\Delta S_{TR}(\text{dTTP}) = -32.32 \pm 11.64$  J/molK; the standard deviation is given as a range.

## SUPPORTING FIGURES

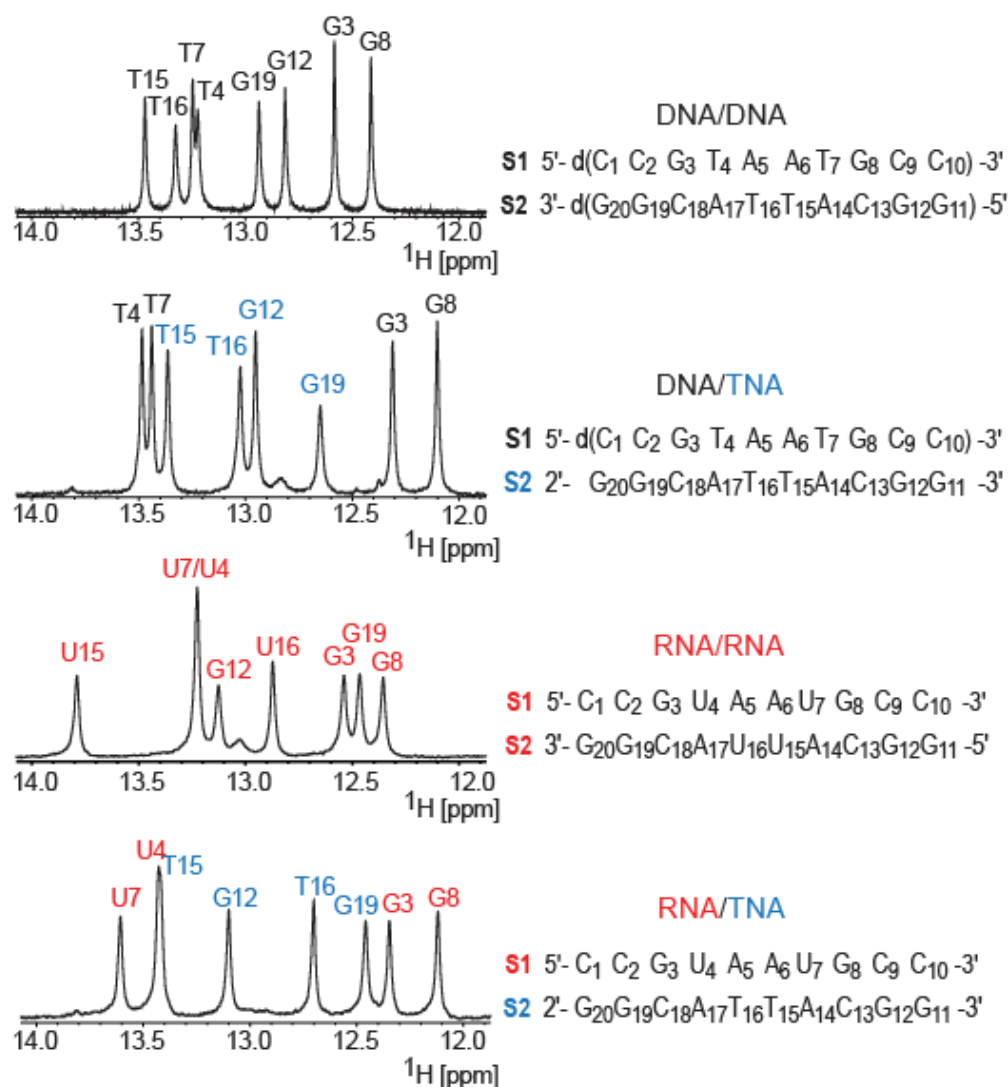


**Figure S1. Oligonucleotide constructs employed in the study.** Left: <sup>1</sup>H imino proton NMR spectra of the constructs studied at 15 °C in aqueous buffer. Proton assignments are shown above the corresponding peaks. Right: sequences of the corresponding duplexes. Names, assignments and strand identifies are color coded according to the nucleic acid of origin: DNA (black), TNA (blue) and RNA (red). Imino proton NMR data clearly shows that TNA forms standard Watson-Crick paired duplexes with DNA and RNA.

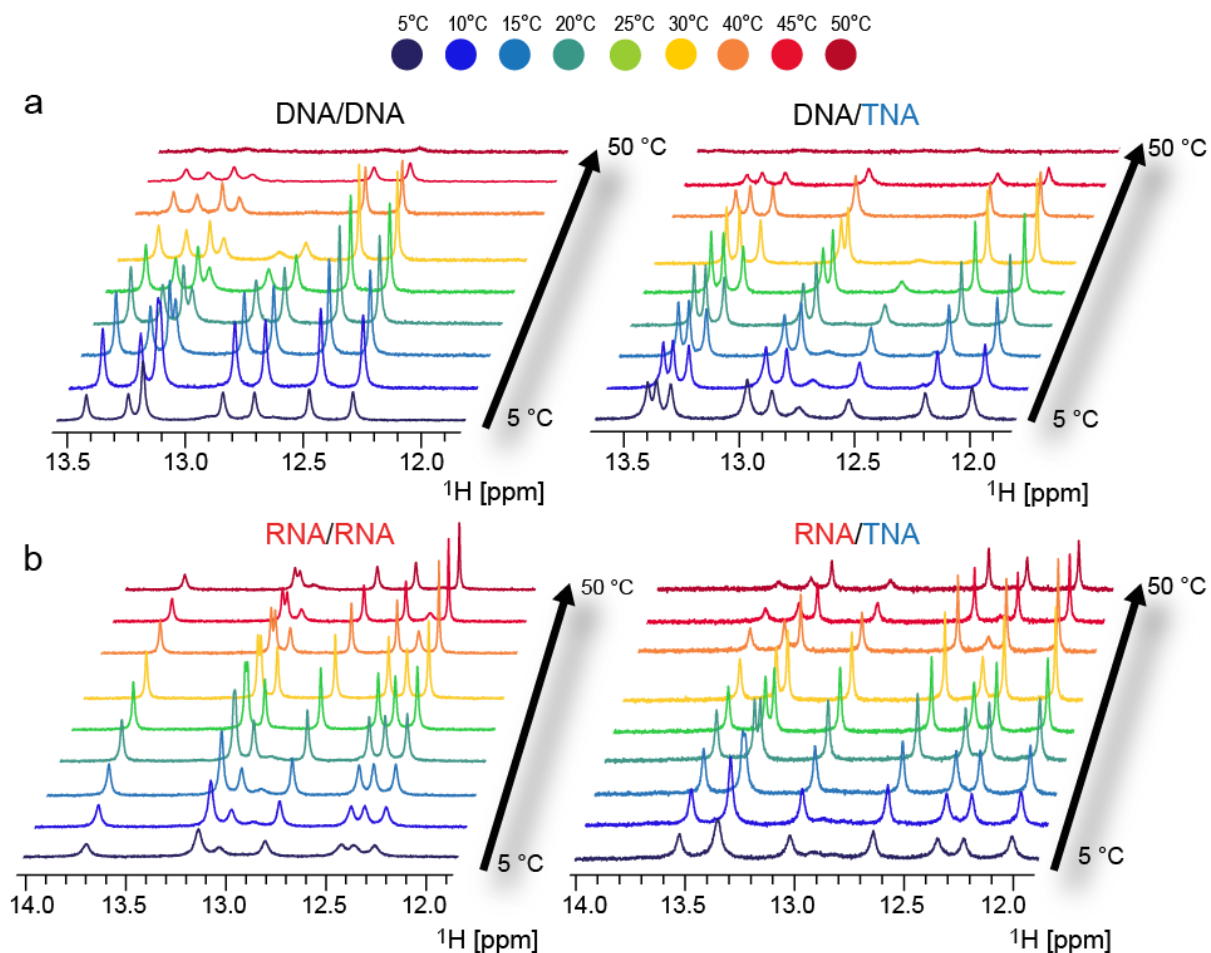


**Figure S2. Temperature-dependent analysis of imino proton region of the natural and TNA chimeric double helices by one-dimensional  $^1\text{H}$  NMR.** (a) DNA-based helices DNA/DNA (left panel), DNA/TNA (right panel). (b) RNA-based helices: RNA/RNA (left panel). RNA/TNA (right panel). All spectra were acquired on Bruker 850 MHz spectrometer 32 scans and 16384 points in direct dimension. The temperature was calibrated using 99.8 % methanol- $d_4$  as described in methods. Receiver gain was kept constant within a set.

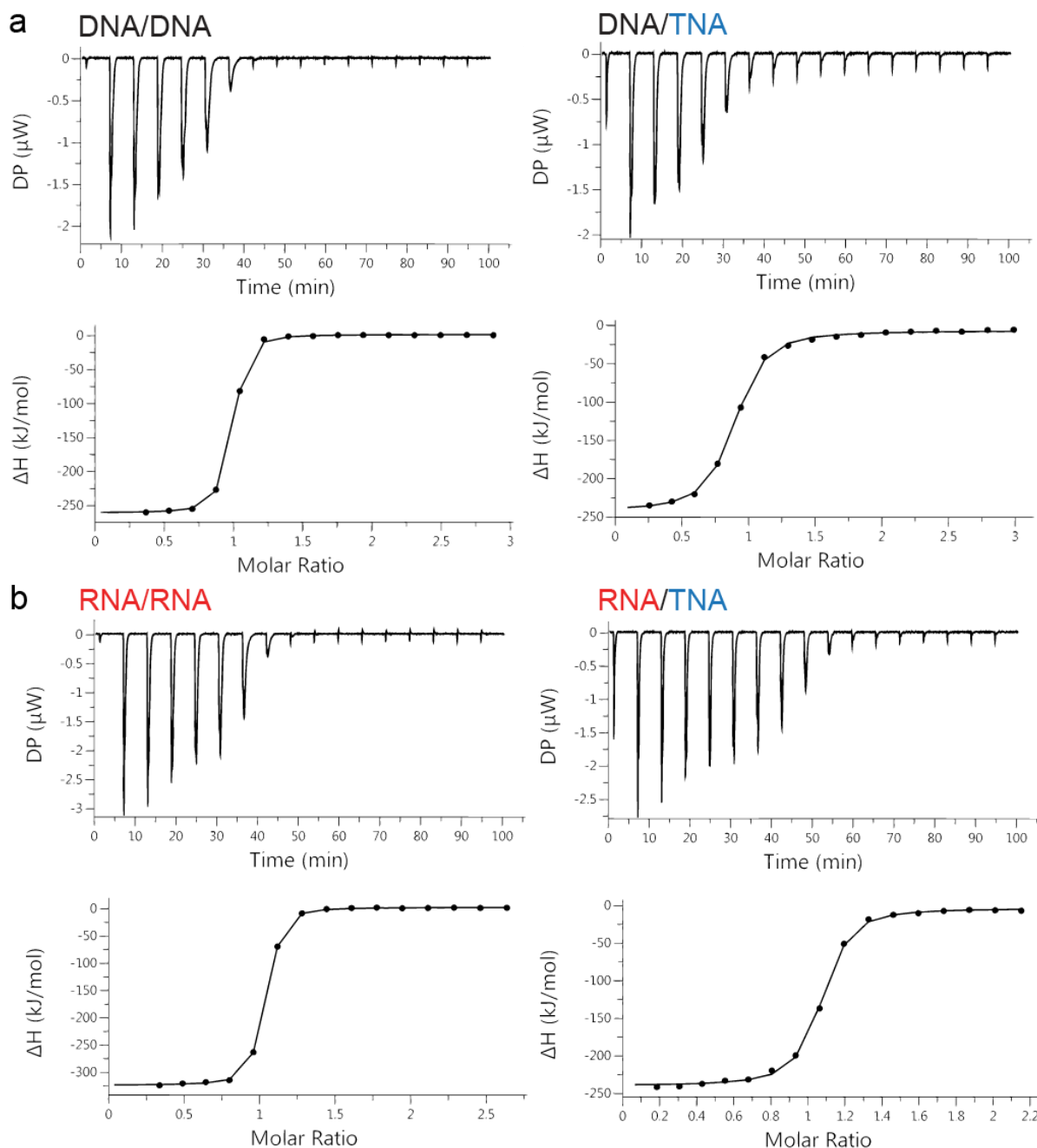


**Figure S3. ITC profiles for the duplex formation of natural helices and chimeras with TNA** (a) Representative ITC profiles for DNA/DNA (left panel) and DNA/TNA (right panel) the duplex formation at 25 °C. (b) ITC profiles for the RNA/RNA (left panel) and RNA/TNA (right panel) duplex formation at 25 °C. Top panels in each case show raw heats of binding (DP) upon sequential injection of 2.4  $\mu\text{L}$  aliquots of solution of one strand to 200  $\mu\text{L}$  of solution of the complementary strand. Lower panels show the enthalpy of interaction ( $\Delta\text{H}$ ) obtained through integration of data (black circles) with binding isotherms fitted to it using one set of sites model.

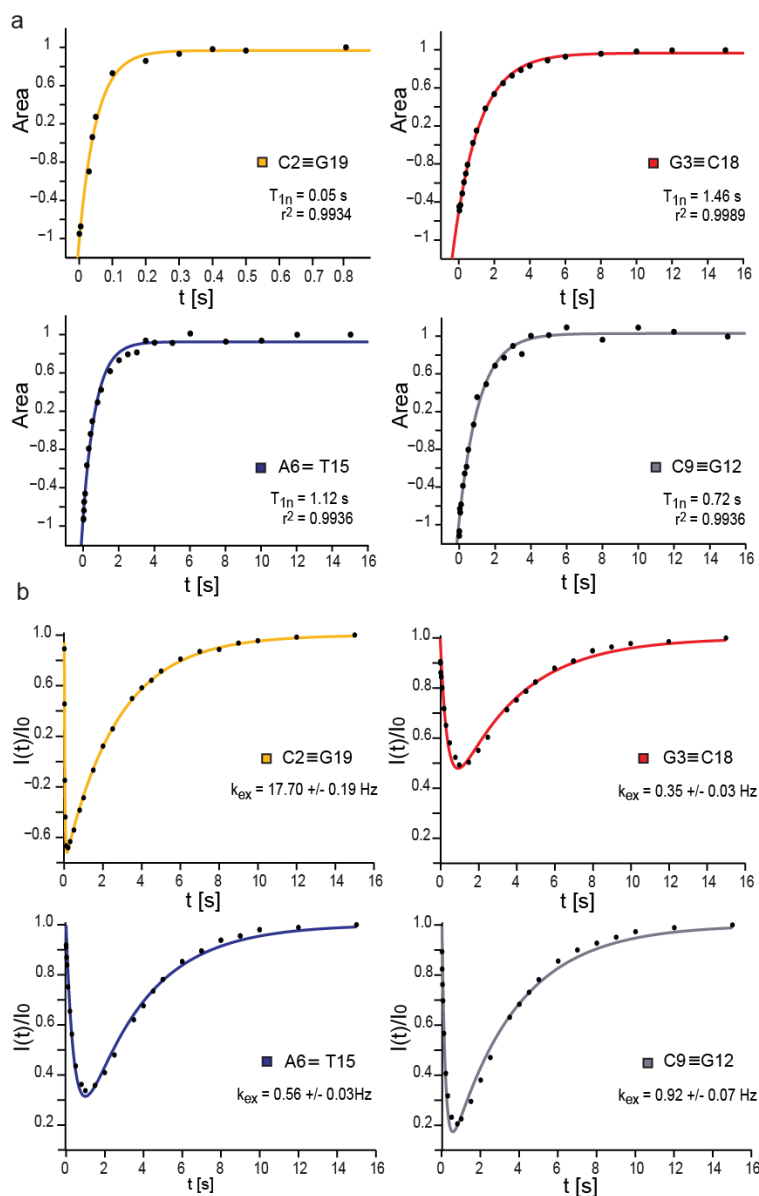


**Figure S4. Examples of data and model fits for analysis of DNA/TNA single basepair exchange rates at 20 °C.** Data points are represented by black circles; the fits are shown by a line of corresponding color. (a) To obtain longitudinal relaxation times for each imino proton, the area under respective imino peaks ( $A$ ) was plotted against the relaxation time delay ( $t$ ) and fitted to the relaxation equation (3), described above. The data fits very well to the negative exponential model. The quality of the fit is reported as  $r^2$ . The obtained longitudinal relaxation time for the base pair ( $T_{1n}$ ) is indicated under each curve. (b) The relative intensity of imino proton signals ( $I(t)/I_0$ ) for the same base pairs as in (a), where  $I(t)$  is the intensity of the peak at delay time  $t$  and  $I_0$  is the intensity of the peak at equilibrium, is plotted against the inversion recovery delay ( $t$ ). Individual base pair exchange rates ( $k_{ex}$ ), obtained from nonlinear fit of the data to equation (5) described above, are indicated under each curve. The errors on the fit are given as a range.

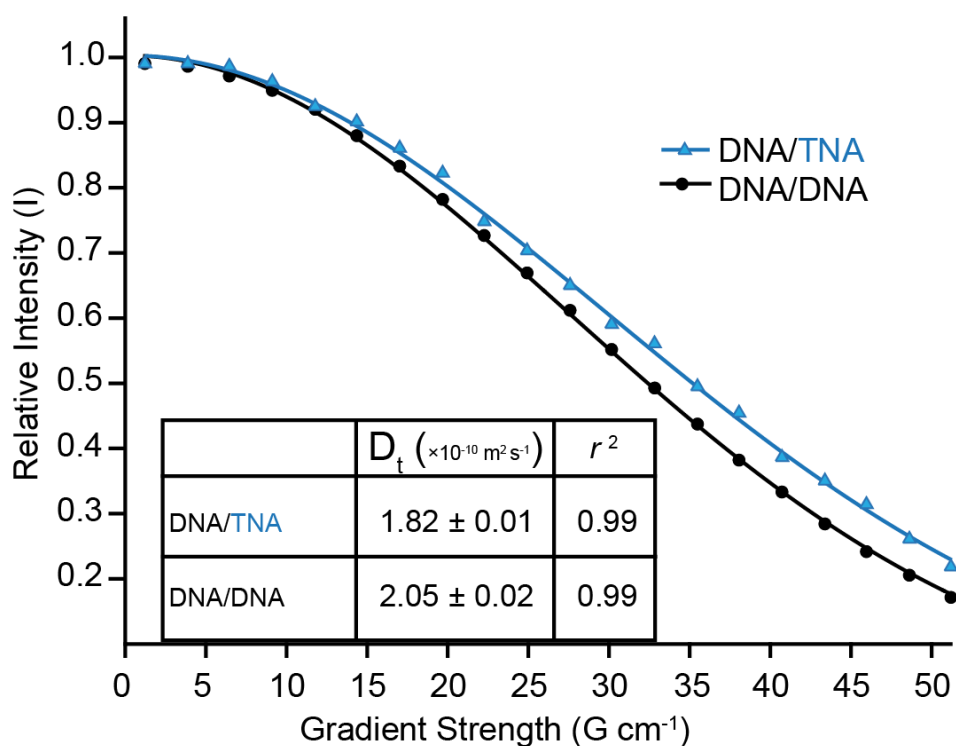


**Figure S5. Diffusion coefficients of DNA/DNA and DNA/TNA duplexes determined by NMR.** Relative peak intensities are plotted against the gradient strength and fit to the Stejskal-Tanner equation<sup>[8]</sup> relating signal intensity ( $I$ ) to the translational diffusion coefficient ( $D_t$ ) as described above. The data points are shown as black circles for DNA/DNA and blue triangles for DNA/TNA, the fit is shown as a line of corresponding color. The data fits very well to the Gaussian shape of the equation and correlates to  $D_t$  of  $1.82 \pm 0.01 \times 10^{-10} \text{ m}^2 \text{ s}^{-1}$  for DNA/TNA, and  $D_t$  of  $2.05 \pm 0.02 \times 10^{-10} \text{ m}^2 \text{ s}^{-1}$  for DNA/DNA with standard deviations from errors on the fit reported as a range. The quality of the fit is reported as  $r^2$ . The data suggests that both molecules diffuse as single duplexes. The DNA/TNA heteroduplex diffuses clearly slower than the DNA/DNA homoduplex, which may be due to the increased intramolecular dynamics of the DNA/TNA, reflected in its slightly bigger apparent shape.

## REFERENCES

- [1] a) S. P. Sau, N. E. Fahmi, J. Y. Liao, S. Bala, J. C. Chaput, *J. Org. Chem.* **2016**; b) S. Zhang, J. C. Chaput, *Curr. Protoc. Nucleic Acid Chem.* **2012**, Chapter 4, Unit 4 51.
- [2] M. Findeisen, T. Brand, S. Berger, *Magn. Reson. Chem.* **2007**, 45, 175-178.
- [3] B. Furtig, C. Richter, J. Wohnert, H. Schwalbe, *ChemBioChem* **2003**, 4, 936-962.
- [4] R. Boelens, R. M. Scheek, K. Dijkstra, R. Kaptein, *J. Magn. Reson.* **1985**, 62, 378-386.
- [5] J. Cavanagh, W. J. Fairbrother, A. G. Plamer III, M. Rance, N. Skelton, *Protein NMR Spectroscopy. Principles and Practice.*, Elsevier, Academic Press, Amsterdam, Boston, Heidelberg, London, New York, Oxford, Paris, San Diego, San Francisco, Singapore, Sydney, Tokyo, **2007**.
- [6] G. Varani, F. Aboul-ela, F. H. T. Allain, *Prog. Nucl. Magn. Reson. Spectrosc.* **1996**, 29, 51-127.
- [7] K. Wuethrich, *NMR of Proteins and Nucleic Acids*, John Wiley & Sons, Inc., United States of America, Canada, **1986**.
- [8] E. O. Stejskal, J. E. Tanner, *J. Chem. Phys.* **1965**, 42, 288-+.
- [9] M. W. Szulik, M. Voehler, M. P. Stone, *Curr. Protoc. Nucleic Acid Chem.* **2014**, 59, 7 20 21-27 20 18.
- [10] a) J. Rinnenthal, B. Klinkert, F. Narberhaus, H. Schwalbe, *Nucleic Acids Res.* **2010**, 38, 3834-3847; b) H. S. Steinert, J. Rinnenthal, H. Schwalbe, *Biophys. J.* **2012**, 102, 2564-2574; c) D. Wagner, J. Rinnenthal, F. Narberhaus, H. Schwalbe, *Nucleic Acids Res.* **2015**, 43, 5572-5585.
- [11] M. Gueron, M. Kochoyan, J. L. Leroy, *Nature* **1987**, 328, 89-92.